RSC Advances

PAPER

View Article Online
View Journal | View Issue

Check for updates

Cite this: *RSC Adv.*, 2026, **16**, 8861

Synergistic modulation of ABC transporter-mediated multidrug resistance by *Kalanchoe laciniata* (L.) DC. phytochemicals: integrative phytochemical profiling, network pharmacology, and molecular docking insights

Anish Ruban S., Francis Jegan Raj, Vetri Velavan Sundararajan and Parimelazhagan Thangaraj *

Kalanchoe laciniata (L.) DC. is an underexplored medicinal plant with promising anticancer potential. This study evaluated the phytochemical profile, antioxidant activity, and multidrug resistance (MDR) modulating effects of its methanolic extract (KLM), with emphasis on ABC transporter regulation. Soxhlet methanol extraction yielded the highest phenolic and tannin contents and exhibited strong antioxidant activity. GC-MS and LC-MS analyses identified bioactive flavonoids and phytosterols, including quercetin and kaempferol derivatives. Network pharmacology revealed key interactions with ABC transporters and hub genes such as AKT1 and TP53. Molecular docking and dynamics simulations demonstrated stable binding of KLM-derived flavonoids with BCRP, MRP1, and AKT1, supporting their role in MDR modulation. Functionally, KLM exhibited dose-dependent cytotoxicity against MDA-MB-231 breast cancer cells and showed strong synergy with doxorubicin. qPCR analysis further confirmed significant downregulation of AKT1, BCRP, and MRP1 expression following KLM treatment. Collectively, these findings indicate that *K. laciniata* phytochemicals may act as effective chemosensitizing agents to overcome ABC transporter-mediated drug resistance in breast cancer.

Received 13th December 2025
Accepted 9th February 2026

DOI: 10.1039/d5ra09649a

rsc.li/rsc-advances

Open Access Article. Published on 13 February 2026. Downloaded on 4/5/2026 6:05:47 PM.
This article is licensed under a Creative Commons Attribution-NonCommercial 3.0 Unported Licence.

Introduction

The genus *Kalanchoe* is a hidden repository of underutilized plants with multiple useful secondary metabolites with significant antioxidant potential. *Kalanchoe laciniata*, commonly referred to as the "Christmas Tree Plant" is a succulent perennial plant belonging to the family Crassulaceae. Known for its strikingly lobed leaves and yellow to orange flowers, *K. laciniata* has gained recognition not only as an ornamental plant but also for its traditional medicinal uses in various cultures from Brazil and Madagascar to parts of Asia.[1] This genus is widely employed in ethnomedicine, where it is used to treat ailments such as inflammation, wounds, coughs, and fever.[2] Its applications in folk medicine have spurred interest in scientific research, leading to investigations into its phytochemical composition and pharmacological potential.[3]

Plant-derived natural compounds have long served as a vital source of therapeutic agents, especially in cancer treatment. These phytochemicals including alkaloids, flavonoids, terpenoids, phenolic compounds, and saponins exhibit a widespread range of biological activities, such as antioxidant, anti-inflammatory, and cytotoxic effects. Several of the most effective anticancer drugs, such as paclitaxel (Taxol) and vincristine, originate from plants, underscoring their potential to provide novel mechanisms for targeting cancer cells.[4,5]

In cancer therapy, either inherent or acquired drug resistance remains a significant challenge. Cancer cells often develop resistance to conventional treatments, such as chemotherapy and targeted therapies, through mechanisms like increased drug efflux, enhanced DNA repair, and evasion of apoptosis.[6,7] This resistance limits treatment efficacy and contributes to disease progression. Plant-derived compounds, with their structural diversity and ability to modulate multiple biological pathways, are emerging as powerful tools in addressing drug resistance in cancer.[8] Drug resistance in cancer is mediated through several mechanisms, one of the most prominent being the over-expression of ATP-binding cassette (ABC) transporters, such as BCRP and MRP1, which actively pump therapeutic drugs out of cancer cells.[9] Phytochemicals like flavonoids and alkaloids have been shown to inhibit these pumps, increasing the intracellular concentration of chemotherapeutic agents.[10] Although drug efflux pumps are only one way through which drug resistance is incurred in plants it plays an important role in the occurrence of drug resistance in cancer cells. In most resistant cells drug efflux transporters are always overexpressed, leading to the efflux of chemotherapeutic drugs.[11]

Bioprospecting Laboratory, Department of Botany, Bharathiar University, Coimbatore 641046, Tamil Nadu, India. E-mail: drparimel@gmail.com

© 2026 The Author(s). Published by the Royal Society of Chemistry

Open Access Article. Published on 13 February 2026. Downloaded on 4/5/2026 6:05:47 PM. This article is licensed under a Creative Commons Attribution-NonCommercial 3.0 Unported Licence.

Although several *Kalanchoe* species, including *K. pinnata* and *K. daigremontiana*, have been reported to exhibit antioxidant, cytotoxic, and pro-apoptotic activities, these studies are largely phenomenological and rarely extend to pathway-level or target-specific mechanistic validation.[12–14] In the context of multidrug resistance (MDR), flavonoids such as quercetin and kaempferol are well known to modulate ABC transporters, particularly P-glycoprotein (ABCB1), MRP1 (ABCC1), and BCRP (ABCG2), through direct binding, ATPase modulation, or transcriptional regulation; however, this evidence predominantly originates from isolated compounds or unrelated botanical sources rather than from other *Kalanchoe* species.[15–17] Importantly, for *Kalanchoe laciniata*, neither the phytochemical landscape nor the systems-level mechanistic links between its endogenous metabolites and MDR-associated targets have been comprehensively investigated. The present study addresses this gap by employing an integrative, multi-scale strategy that combines phytochemical profiling with network pharmacology, molecular docking, and molecular dynamics simulations to systematically interrogate how *K. laciniata* derived compounds interact with key ABC transporters and cancer-associated proteins. By contextualizing known flavonoid–transporter interactions within the species-specific and combinatorial synergism of *K. laciniata*, this work advances beyond activity-based observations and provides mechanistic evidence for the potential modulation of ABC transporter mediated drug efflux and interconnected MDR pathways, thereby establishing a distinct mechanistic framework for this underexplored species.

Materials and methods

Chemical and reagents

Methanol (67-56-1), petroleum ether (8032-32-4), and ethyl acetate (141-78-6) were procured from Merck (Darmstadt, Germany). Dimethyl sulfoxide (DMSO; 67-68-5), Folin–Ciocalteu's reagent (8024-55-5), DPPH (2,2-diphenyl-1-picrylhydrazyl; 1898-66-4), aluminum chloride (7446-70-0), sodium carbonate (497-19-8), potassium acetate (127-08-2), and all positive controls were obtained from Sigma-Aldrich Chemical Co. (St. Louis, MO, USA).

Sample collection

Kalanchoe laciniata plant samples were gathered from the Western Ghats in the Theni district. The collected plants were thoroughly cleaned, shade-dried separately, and then ground. The sample was authenticated and certified by the Botanical Survey of India, Southern Regional Centre, Coimbatore (BSI/SRC/5/23/2023-24/Tech/58). The plant material was shade-dried for six weeks, after which it was ground into a fine powder. The literature study was conducted for different parts of *Kalanchoe laciniata* and the entire plant part was chosen for its maximum antioxidant and phytochemical potential.

Phytochemical extraction

Plant material (50 g) was extracted using petroleum ether, ethyl acetate, methanol, and water through two methods: cold maceration and Soxhlet extraction. For cold maceration, the powdered sample was soaked in 300 mL of each solvent for 48 hours at room temperature, after which the extracts were filtered and concentrated under reduced pressure at 50 °C. For Soxhlet extraction, 50 g of plant material was continuously extracted with 300 mL of each solvent at their respective boiling points for 4–8 hours to ensure efficient recovery of phytochemicals. All extracts were concentrated under vacuum and stored for further analysis.[18,19]

Secondary metabolite quantification

The total phenolic content (TPC), total flavonoid content (TFC), and total tannin content (TTC) of the plant extracts were quantified using five different solvent extracts. TPC and TTC were determined using the Folin–Ciocalteu method. For TPC, extract solutions (1 mg per mL stock) were reacted with the reagent, and absorbance was recorded at 725 nm, with results expressed as mg gallic acid equivalents (GAE)/g dry weight. TTC was measured similarly, with tannins removed using PVPP to obtain non-tannin phenolics. Tannin content was calculated as:

$$\text{Tannins (g)} = \text{total phenolics (g)} - \text{non-tannin phenolics (g)}.$$

TFC was assessed using the aluminum chloride colorimetric method, with absorbance measured at 510 nm and results expressed as mg rutin equivalents (RUE)/g dry weight.[20,21]

In vitro antioxidant assays

The antioxidant potential of the plant extracts was evaluated using multiple *in vitro* assays. DPPH radical scavenging activity was determined by reacting various extract concentrations (final volume 100 μL) with DPPH solution, using BHT and rutin as positive controls. The decrease in absorbance at 517 nm indicated radical scavenging, and IC_{50} values were calculated.[22] Ferric Reducing Antioxidant Power (FRAP) was measured by the reduction of the Fe^{3+}–TPTZ complex to Fe^{2+}, forming a violet chromophore with absorbance recorded at 593 nm, expressed as Fe(II) equivalents.[23]

For phosphomolybdenum activity, extracts reduced Mo(VI) to Mo(V), generating a green complex measured at 695 nm, with results expressed as ascorbic acid equivalents (AAE).[24] ABTS scavenging activity was quantified by reacting extracts with $ABTS^{+}$ solutions for 30 minutes and measuring absorbance at 734 nm. Antioxidant capacity was expressed as Trolox equivalence, and IC_{50} values were calculated.[25] Superoxide radical scavenging activity was assessed using the riboflavin-light-NBT system, where inhibition of formazan formation was measured at 590 nm and expressed as percentage inhibition compared to control.[26]

Characterization of secondary metabolites

GC-MS analysis. GC-MS profiling was performed using a PerkinElmer Clarus SQ8C system. The injector, interface, and ion source temperatures were set at 230 °C, 260 °C, and 200 °C, respectively. The oven was programmed from 70 °C (5 min) to 120 °C at 5 °C min^{-1}, then to 290 °C at 8 °C min^{-1}. Samples

 © 2026 The Author(s). Published by the Royal Society of Chemistry

Open Access Article. Published on 13 February 2026. Downloaded on 4/5/2026 6:05:47 PM. This article is licensed under a Creative Commons Attribution-NonCommercial 3.0 Unported Licence.

were injected in split mode (1 : 50) and separated on an Agilent DB-35 MS column using helium (1 mL min^{-1}). Mass spectra were acquired from 50–650 Da at −70 eV. Compounds were identified by comparison with NIST4 and WILEY9 libraries, considering matches with spectral fit values > 700.[27]

LC-MS analysis. LC-MS analysis was performed using a Shimadzu LCMS-8030 triple quadrupole mass spectrometer equipped with an electrospray ionization (ESI) source. Chromatographic separation was achieved on an Acquity UPLC BEH C18 column using a binary mobile phase consisting of water with 0.1% formic acid (A) and acetonitrile with 0.1% formic acid (B), with a gradient of 5–95% B over 18 min, held at 95% B for 4 min, and re-equilibrated to initial conditions, at a flow rate of 0.3 mL min^{-1} and column temperature of 40 °C. The sample was injected at a volume of 5 μL. Mass spectrometric detection was conducted in both positive and negative ion modes with an interface voltage of ±4.5 kV, nebulizing gas flow of 3.0 L min^{-1}, drying gas flow of 10 L min^{-1}, and desolvation line temperature of 250 °C, acquiring full-scan spectra over an m/z range of 100–1000. Raw data was preprocessed and the mass spectrum was then again analyzed using the two reference libraries – NIST4 and WILEY.[28]

Network pharmacology

Construction and screening of KLM phytochemicals and target databases. LC-MS and GC-MS analysis of the KLM revealed a diverse array of bioactive compounds with potential therapeutic effects. SMILES structures of compounds identified *via* GC and LC analyses were retrieved from the PubChem database and used to predict target genes through the Swiss Target Prediction tool. Protein targets were further validated by confirming their UniProtKB IDs. Key pharmacokinetic parameters were evaluated using SwissADME and MolSoft online platforms. Additionally, toxicity classes were predicted using the Protox web tool.[29] To identify disease-associated targets, the keywords "ABC Transporters" and "Drug-Resistant Genes" were searched in GeneCards and OMIM. Targets from both databases were compiled, standardized by gene name, and duplicates removed.

Compound–target and protein–protein interaction (PPI) network construction. Compound–target associations were visualized using Cytoscape 3.10.3 and analyzed using its Network Analysis tool to obtain topological parameters such as degree, betweenness centrality, compactness, and average shortest path length. A Venn diagram was used to identify overlapping genes between phytochemical targets and ABC transporter-associated genes. The common genes were subjected to PPI analysis using STRING 12.0, and the resulting network was imported into Cytoscape. Hub genes were identified using CytoHubba (degree algorithm), and major gene modules were detected using MCODE.[30]

KEGG pathway and GO gene enrichment analysis. The analysis employed multiple biological databases to investigate cellular components (CC), molecular functions (MF), and biological processes (BP) within extensive genetic datasets. Gene Ontology (GO) enrichment analysis provided insights into gene functions, pathways, and cellular localization, using tools such as STRING 12.0 and ShinyGO.[31] For pathway network mapping, the top 20 KEGG pathways were imported into Cytoscape, and a comprehensive pathway-target network was constructed. Network analysis metrics (degree, BC, CC, ASPL) were calculated to determine core pathways and their central targets.[30]

***In silico* docking of compounds against ABC transporter proteins.** Protein structures corresponding to the selected targets (AKT1, TNF-A, TP53, ALB, P-gp, BCRP, and MRP1; PDB IDs 6HHG, 6RMJ, 7VR0, 8DC4, 7O9W, 6VXI, and 4C3Z) were retrieved from the RCSB Protein Data Bank and pre-processed using the Protein Preparation Wizard in Schrödinger Maestro. This step corrected bond orders, added missing atoms and hydrogens, assigned formal charges, and optimized the structures for docking. Ligands were prepared using LigPrep to generate energy-minimized, all-atom 3D structures from the initial 2D/3D input files.[32]

Receptor grids were then generated for each target using the Receptor Grid Generation tool, with the active site defined based on the co-crystallized ligand or known binding region. Grid parameters were optimized through the receptor, site, constraints, and rotatable groups tabs to ensure accurate docking. Prepared ligands were subsequently docked into the generated grids using glide in extra precision (XP) mode. Docking scores and binding interactions were analyzed, and protein–ligand complexes were visualized using both 2D and 3D interaction diagrams.[33]

Molecular dynamics (MD) simulation analysis. Desmond (Schrödinger Suite, version 4.1) was used to assess the conformational stability of receptor–ligand complexes through 100 ns molecular dynamics (MD) simulations. Three ABC transporter–ligand complexes and one hub gene–ligand complex were simulated. Stability and behavior were evaluated using RMSD, RMSF, protein–ligand contact analysis, and hydrogen bond monitoring throughout the simulation.[34]

Maestro was used to prepare protein–ligand complexes and refine side-chain residues before MD simulation (Schrödinger, LLC, 2019-2). Desmond added missing atoms and applied the TIP3P water model for solvation. An orthorhombic box (10 × 10 × 10 Å) was created around the complex, and Na^+ and Cl^- ions were added to neutralize the system. To mimic physiological conditions, 0.15 M NaCl was included during a 100 ns NPT simulation at 310 K and 1 bar, with data recorded every 10 ps. Systems were energy-minimized using Desmond's relaxation module (1 kcal per mol convergence, 2000 iterations) and pre-equilibrated before simulation. The OPLS_2005 force field and SPC solvent model were employed throughout.[35]

Cell growth and cytotoxicity analysis. MDA-MB-231 (human breast cancer) and RIN5F (normal pancreatic β-cell) lines were procured from NCCS (Pune, India) and cultured in DMEM supplemented with 10% FBS and 1% penicillin–streptomycin at 37 °C in 5% CO_2. Upon reaching confluence, cells were trypsinized and seeded in 96-well plates (5000 cells per well).

Cytotoxicity of KLM was assessed using the MTT assay after 24 h treatment. RIN5F cells were exposed to 100–600 μg mL^{-1}, and MDA-MB-231 cells to 10–100 μg per mL extract. Doxorubicin (1.5 μM) served as the positive control. The MTT assay was

Open Access Article. Published on 13 February 2026. Downloaded on 4/5/2026 6:05:47 PM. This article is licensed under a Creative Commons Attribution-NonCommercial 3.0 Unported Licence.

performed following a reagent-based colorimetric protocol adapted from previously published literature,[36] which has been routinely used to assess cytotoxic effects of bioactive compounds in cultured cells. Following treatment, MTT solution (5 mg mL^{-1}; 20 μL per well) was added to the cultures and incubated at 37 °C for 4 h to allow for formazan crystal formation. The resulting insoluble formazan was subsequently solubilized using DMSO, and absorbance was recorded at 570 nm. Cell viability was calculated and expressed as a percentage relative to untreated control cells.

For cell death visualization, propidium iodide (PI) staining was performed under identical treatment conditions. Following exposure, cells were washed with phosphate-buffered saline (PBS), incubated with PI solution (10 μg mL^{-1}) for 5–10 min at room temperature in the dark, and immediately visualized under an inverted EVOS fl AMG. In addition, bright-field images of RIN5F cells were acquired using the same microscope. The same conditions were followed for RNA extraction from extract-treated cells and further used for RT-qPCR analysis.

Combination index (CI). The combination index (CI) provides a quantitative measure of the extent of interaction between two agents at a defined level of biological effect. In this study, the CI was used to evaluate the interaction between KLM and doxorubicin (DOX) in MDA-MB-231 human breast cancer cells. The analysis was based on the median-effect principle and Chou–Talalay method.[37]

Cells were treated with various concentrations of *K. laciniata* extract and DOX individually, as well as in fixed-ratio combinations derived from their respective IC_{50} values. After 24 hours of exposure, cell viability was assessed using the MTT assay as described above, and the percentage inhibition values were used for CI calculation.

The combination index (CI) was calculated using the equation:

$$\mathrm{CI} = \frac{D_1}{Dx_1} + \frac{D_2}{Dx_2}$$

where: D_1 = concentration of *K. laciniata* extract in combination required to achieve a specific effect (*e.g.*, 50% inhibition), D_2 = concentration of doxorubicin in combination required to achieve the same effect, Dx_1 = concentration of *K. laciniata* extract alone producing that effect, and Dx_2 = concentration of doxorubicin alone producing that effect.

RNA isolation, cDNA synthesis, and quantitative real-time PCR analysis. MDA-MB-231 breast cancer cells were treated with KLM extract (IC_{50} concentration) for 24 h. Total RNA was isolated using TRIzol™ reagent (Invitrogen, USA). Briefly, cells were washed twice with ice-cold PBS, lysed with 1 mL TRIzol in 6-well plates, and homogenized by pipetting. Chloroform (200 μL) was added, and samples were centrifuged at 12 000 × *g* for 15 min at 4 °C. The aqueous phase was transferred to a fresh tube, and RNA was precipitated with isopropanol, followed by centrifugation at 12 000 × *g* for 10 min at 4 °C. The RNA pellet was washed with 75% ethanol, air-dried, dissolved in RNase-free water, and quantified using a NanoDrop spectrophotometer. RNA samples were stored at −80 °C until use. cDNA was synthesized from 1 μg total RNA using the Bio-Rad iScript™ cDNA Synthesis Kit in a 20 μL reaction volume following the manufacturer's instructions. Reverse transcription was performed at 25 °C for 5 min, 46 °C for 20 min, and 95 °C for 1 min. The resulting cDNA was stored at 20 °C. Quantitative real-time PCR was performed using iTaq™ Universal SYBR® Green Supermix (Bio-Rad, USA) on a Bio-Rad CFX Opus system. Each 20 μL reaction contained SYBR Green master mix, gene-specific primers, and diluted cDNA. The primers used were β-actin – forward: 5′-AGAGCTACGAGCTGCCTGAC-3′, reverse: 5′-AGCACTGTGTTGGCGTACAG-3′; AKT1 – forward: 5′-GCTGCTGCTGAGGAGAAACT-3′, reverse: 5′-TGAGGA-CAGGATGAGGAGGA-3′; BCRP – forward: 5′-CAGTGGA-GAGGAGGACATCA-3′, reverse: 5′-TCTCCTGCTGCTGATGGTAA-3′; PGP – forward: 5′-ATGGTGCTGGAAGGAGACAA-3′, reverse: 5′-CTCAGGGTGGTGATGGTGTA-3′; and MRP1 forward: 5′-TGCTGGAGCTGTTTGATGAA-3′, reverse: 5′-TTTGGTGGTGGTGTCTGTCT-3′. Reactions were run in duplicate under the following conditions: 95 °C for 3 min, followed by 40 cycles of 95 °C for 10 s and 60 °C for 30 s. Melt curve analysis was performed to confirm amplification specificity. Relative gene expression was normalized to β-actin and calculated using the $2^{-\Delta\Delta C_t}$ method, with results expressed as fold change relative to the control.[36,38]

Statistical analysis. Results were expressed as the mean ± SD of three replicates. One-way ANOVA followed by Duncan's multiple range test was used to determine significant differences ($p < 0.05$) using GraphPad software (version 10.2.0.).[39]

Results

Extraction and quantification of secondary metabolites

The powdered plant (50 g) was extracted using four different solvents using two different extraction methods, Soxhlet and cold maceration. Non-polar to polar solvents were used (petroleum ether, ethyl acetate, methanol, and water) (300 mL). The extract was concentrated to dryness under reduced pressure in a rotary evaporator to yield dried extracts. Further, yield extract was calculated and the dried extracts were used for the follow-up studies.

Secondary metabolites, including TPC, TFC, and TTC contents of *Kalanchoe laciniata* extracts, were analyzed. The total phenolic content, assessed using the Folin–Ciocalteu method and expressed as gallic acid equivalents (GAE), was highest in the Soxhlet methanol extract (278.98 ± 0.65[a] mg GAE per g extract). Similarly, the total flavonoid content, determined using the aluminum chloride method and expressed as rutin equivalents (RE), peaked in the macerated methanol extract (371.32 ± 45.73[a] mg RE/g extract). Total tannin content, calculated by subtracting non-tannin phenolics from the total phenolics and expressed as GAE, was also highest in the Soxhlet methanol extract (55.39 ± 1.46[a] mg GAE/g extract). These findings suggest that Soxhlet extraction is the most effective method, and methanol is the most suitable solvent for isolating secondary metabolites from *K. laciniata* Table 1.

Antioxidant assays. The antioxidant activities of *Kalanchoe laciniata* extracts were evaluated using various *in vitro* assays, consistently identifying the methanol extract as the best-

 © 2026 The Author(s). Published by the Royal Society of Chemistry

Open Access Article. Published on 13 February 2026. Downloaded on 4/5/2026 6:05:47 PM. This article is licensed under a Creative Commons Attribution-NonCommercial 3.0 Unported Licence.

performing solvent extract. In the DPPH scavenging assay, the Soxhlet methanol extract exhibited the highest activity with an IC_{50} of 11.46 μg mL^{-1}, confirming its strong free radical scavenging capacity. Similarly, in the FRAP assay, the Soxhlet methanol extract demonstrated the greatest ferric-reducing antioxidant power with a value of 971.98 ± 1.15 mmol Fe(II)/mg extract, outperforming all other extracts. The phosphomolybdenum assay further highlighted the Soxhlet methanol extract's superior total antioxidant capacity, expressed as 246.98 ± 22.59 ascorbic acid equivalents per gram. Fig. 1A–C. Across all assays, the Soxhlet methanol extract consistently outperformed other extracts, confirming its efficacy as the most effective solvent and extraction method combination for extracting antioxidants from *Kalanchoe laciniata*. These findings align with prior studies that have highlighted the efficiency of Soxhlet methanol in extracting bioactive compounds due to its polar nature, which facilitates the dissolution of a wide range of antioxidant metabolites.

Characterization of phytocompounds

GC-MS. The Soxhlet methanolic extract of *K. laciniata* was investigated through Gas Chromatography-Mass Spectrometry (GC-MS) analysis. The resulting chromatogram, provided a comprehensive overview of the volatile compounds present in the extract, revealing a total of 22 peaks (Table 2) (Fig. S1). These peaks were analyzed based on their relative retention times (R_t) and mass spectra, compared against the standard NIST library for accurate identification.[40]

Among the identified compounds, octadecadienoic acid, known for its role as a fatty acid with potential health benefits, exhibited the highest peak area percentage of 27.67% at a retention time of 10.98. Additionally, stearic acid, a saturated fatty acid recognized for its moisturizing properties, and pentadecanone, a ketone that may possess antimicrobial activity, were also prominent in the extract. Furthermore, the analysis revealed the presence of quercetin derivatives, which are known for their antioxidant properties, as well as various phytol groups and other phenolic compounds that contribute to the plant's bioactivity.

The compounds detected in the GC-MS analysis are associated with significant biological and medicinal properties, although many of their specific activities remain to be fully explored. This analysis underscores the potential therapeutic applications of *K. laciniata* based on its rich profile of biactive compounds.

LC-MS. The Liquid Chromatography-Mass Spectrometry (LC-MS) analysis of the Soxhlet methanolic extract from *K. laciniata* identified a total of 15 distinct compounds, utilizing both positive and negative ionization modes. Among these compounds, several notable flavonoid glycosides were detected, including kaempferol 3-*O*-(2′-*O*-D-glucopyranosyl)-beta-D-galactopyranoside, kaempferol-3-*O*-glucoside-3″-rhamnoside, and kaempferol 3-(3″,4″-diacetylrhamnoside). Along with quercetin and kaempferol derivatives, kalanchosides and kalambrosides, which are specific to *Kalanchoe* genus were also identified, highlighting the unique chemical characteristics of this plant. These compounds are significant due to their potential health benefits, including antioxidant and anti-inflammatory properties. The findings from the LC-MS analysis underscore the potential therapeutic applications of *K. laciniata* based on its rich array of bioactive compounds Table 3 (Fig. S2).

Network pharmacology-based analysis

Active chemical compositions and target prediction of KLM. A total of 37 bioactive compounds were identified from the KLM through phytochemical profiling. *In silico* pharmacokinetic screening using the SwissADME platform revealed that 15 compounds exhibited high predicted gastrointestinal absorption. These compounds also demonstrated favorable drug-likeness, showing compliance with key oral drug-likeness criteria, including Lipinski's Rule of Five and Veber parameters related to molecular weight, lipophilicity, hydrogen bonding capacity, topological polar surface area, and molecular flexibility. Preliminary toxicity evaluation using the ProTox-II server further indicated that only 14 of these compounds belonged to toxicity classes IV–VI, corresponding to low predicted acute toxicity, and were therefore prioritized for downstream analysis. The potential molecular targets of the selected compounds were subsequently predicted using the SwissTargetPrediction tool, providing a compound–target dataset for network pharmacology analysis and mechanistic exploration.

Table 1 TPC, TFC and tannin content values of various solvent extracts of *K. laciniata* using Soxhlet and cold maceration methods

Method used	Solvent used	Total phenolic content (GAE/g extract)	Total flavonoid content (RE/g extract)	Total tannin content (GAE/g extract)
Soxhlet	Petroleum ether	13.54 ± 1.57^{e}	134.91 ± 10.43^{c}	3.54 ± 0.51^{d}
	Ethyl acetate	81.91 ± 1.94^{c}	258.60 ± 13.26^{b}	9.34 ± 2.97^{b}
	Methanol	$\boldsymbol{278.9815 \pm 0.65^{a}}$	182.28 ± 5.41^{c}	$\boldsymbol{55.39 \pm 1.46^{a}}$
	Water	46.89 ± 5.40^{d}	109.91 ± 0.62^{c}	10.92 ± 1.71^{b}
Macerated	Petroleum ether	10.31 ± 3.21^{e}	258.16 ± 67.68^{b}	1.53 ± 0.19^{c}
	Ethyl acetate	18.64 ± 1.90^{e}	$\boldsymbol{371.32 \pm 45.73^{a}}$	6.23 ± 2.37^{c}
	Methanol	244.41 ± 31.03^{b}	181.40 ± 30.20^{c}	51.97 ± 1.02^{a}
	Water	55.99 ± 3.08^{d}	109.91 ± 1.64^{c}	12.89 ± 0.25^{b}

Different letters within one column indicate a significant difference between treatments n = 3, ($a < b < c < d < e \leq 0.05$) on DMRT analysis. Values consisted of mean ± SD.

© 2026 The Author(s). Published by the Royal Society of Chemistry

Open Access Article. Published on 13 February 2026. Downloaded on 4/5/2026 6:05:47 PM. This article is licensed under a Creative Commons Attribution-NonCommercial 3.0 Unported Licence.

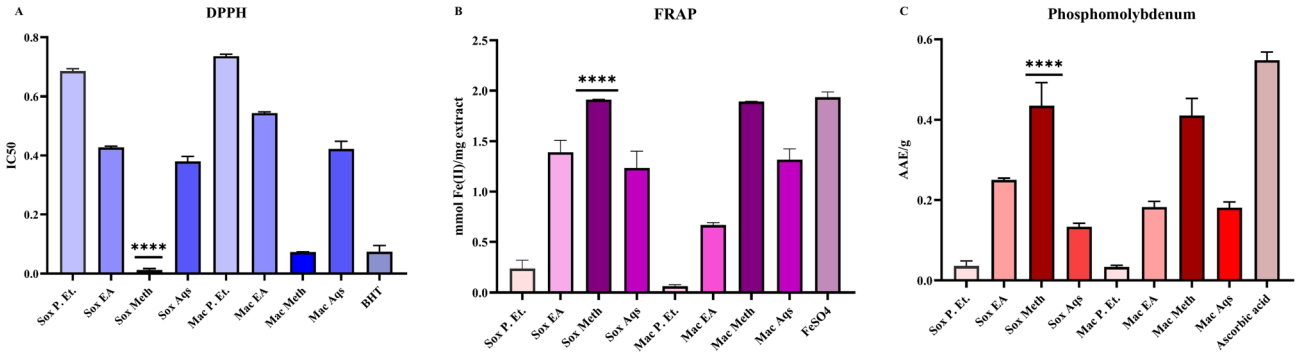

Fig. 1 (A–C) illustrates the (A) DPPH, (B) FRAP, (C) phosphomolybdenum, assay of *K. laciniata* extracts obtained through Soxhlet and cold maceration methods using five different extracts. Data are presented as mean ± standard deviation ($n = 3$). Statistical significance was evaluated using one-way ANOVA followed by post hoc analysis. Groups sharing different superscript letters are significantly different at $p < 0.01$.

Construction of the KLM compounds–target network diagram. Through GC-MS and LC-MS analyses, a total of 14 bioactive compounds that met the screening criteria were identified in the methanolic extract of *K. laciniata*. The potential protein targets of the identified compounds were subsequently predicted using the SwissTargetPrediction online platform, which resulted in 411 ligand-associated targets through network pharmacology analysis.

In parallel, ABC transporter-related target genes were retrieved from publicly available databases, including GeneCards and OMIM. After removal of duplicate entries, a total of 2123 ABC transporter targets were obtained. The intersection between the predicted ligand targets and ABC transporter-associated genes was performed using the online bioinformatics tool Venny, which identified 185 common genes as potential therapeutic targets, as presented in Fig. S3. The ligand–target interaction network consisted of 474 nodes and 1500 edges. The network exhibited a centralization value of 0.199, an average number of neighbors of 6.329, and a characteristic path length of 3.254, indicating a moderately connected biological network.

Construction of PPI network of *K. laciniata* extracts and ABC transporters targets. To explore the relationships among the 320 potential therapeutic targets, the STRING database was utilized to construct a protein–protein interaction (PPI) network. Visualization of the network was performed using

Table 2 Identified metabolites in the methanolic extract of *Kalanchoe laciniata* using GC-MS analysis

S. no.	Retention time	CAS no.	Name	Molecular formula	Molecular weight	Probability%	Peak area
1	7.14	150-86-7	Phytol	$C_{20}H_{40}O$	296	35.45	4.54
2	9.03	112-72-1	1-Tetradecanol	$C_{14}H_{30}O$	214	19.64	0.67
3	10.98	2462-85-3	9,12-Octadecadienoic acid, methyl ester	C19H34O2	294.5	79.45	27.67
4	12.66	519-96-0	Patuletin	$C_{16}H_{12}O$	332	17.37	0.53
5	14.05	88-32-4	3-*tert*-Butyl-4-methoxyphenol	$C_{11}H_{16}O_2$	180	36.78	4.91
6	14.61	818-23-5	8-Pentadecanone	$C_{15}H_{30}O$	226.39	65.57	19.15
7	15.53	628-97-7	Hexadecanoic acid, ethyl ester	$C_{18}H_{36}O_2$	284.47	31.46	1.89
8	15.96	83-48-7	Stigmasterol	$C_{29}H_{48}O$	412.69	23.41	2.05
9	17.24	2363-71-5	Heneicosanoic acid	$C_{21}H_{42}O_2$	326.55	40.15	5.31
10	19.5	7132-64-1	Pentadecanoic acid methyl ester	$C_{16}H_{32}O_2$	256	46.78	6.56
11	22.09	629-94-7	Heneicosane	$C_{21}H_{44}$	296	27.48	0.71
12	24.22	57-10-3	Palmitic acid	$C_{16}H_{32}O_2$	256	37.69	3.84
13	24.98	112-61-8	Stearic acid methyl ester	$C_{19}H_{38}O_2$	298	56.74	14.89
14	27.11	6068-80-0	Quercetin 7,3′,4′-trimethyl ether	$C_{18}H_{16}O_7$	344	17.84	0.59
15	29.68	331-39-5	Caffeic acid	C9H8O4	180	11.65	0.08
16	32.02	111-02-4	Squalene	$C_{30}H_{50}$	410	20.47	0.31
17	35.28	2631-37-0	Phenol, 3-methyl-5-(1-methylethyl)-, methylcarbamate	$C_{12}H_{17}NO_2$	207	16.78	0.09
18	37.16	459-80-3	Geranic acid	$C_{10}H_{16}O_2$	168	24.74	0.21
19	37.93	124-07-2	Octanoic acid	$C_8H_{16}O_2$	144	39.74	2.87
20	38.55	82304-66-3	7,9-Di-*tert*-butyl-1-oxaspiro(4.5)deca-6,9-diene-2,8-dione	$C_{17}H_{24}O_3$	276	19.43	1.93
21	40.08	28564-83-2	2,3-Dihydro-3,5-dihydroxy-6-methyl-4*H*-pyran-4-one	$C_6H_8O_4$	144.12	19.61	0.53
22	41.23	33983-40-3	(+)-Medicarpin	$C_{16}H_{14}O_4$	270.28	22.78	0.61

© 2026 The Author(s). Published by the Royal Society of Chemistry

Open Access Article. Published on 13 February 2026. Downloaded on 4/5/2026 6:05:47 PM. This article is licensed under a Creative Commons Attribution-NonCommercial 3.0 Unported Licence.

Table 3 Identified metabolites in the methanolic extract of *Kalanchoe laciniata* using LC-MS analysis

S. no.	Pubchem ID	Molecular formula	Molecular weight	Compound name
1	49798774	$C_{30}H_{42}O_{10}$	562.6	Kalanchoside C
2	90658606	$C_{27}H_{29}O_{16}^-$	609.5	Kaempferol 3-*O*-(2′-*O*-D-glucopyranosyl)-beta-D-galactopyranoside
3	74124649	$C_{27}H_{30}O_{15}$	594.5	Kaempferol-3-*O*-glucoside-3″-rhamnoside
4	44258959	$C_{25}H_{24}O_{12}$	516.4	Kaempferol 3-(3″,4″-diacetylrhamnoside)
5	11994609	$C_{30}H_{42}O_{10}$	562.6	Kalanchoside B
6	14238625	$C_{27}H_{30}O_{16}$	610.5	Quercetin 3-(2-glucosylrhamnoside)
7	5369484	$C_{31}H_{40}O_{15}$	652.6	Cinnamic acid (compound NP-002173)
8	14189384	$C_{36}H_{58}O_8$	618.8	Oleanolic acid beta-D-glucopyranosyl ester
9	5274585	$C_{21}H_{18}O_{13}$	478.4	Miquelianin
10	129889798	$C1_8H_{16}O_9$	376.3	Tri-(methoxy)-kaempferol
11	5280805	$C_{27}H_{30}O_{16}$	610.5	Rutin
12	16218542	$C_{27}H_{36}O_{19}$	664.6	Rutin trihydrate
13	12366	$C_{18}H_{36}O_2$	284.5	Ethyl palmitate
14	5274586	$C_{26}H_{28}O_{16}$	596.5	Quercetin 3-*O*-beta-D-xylopyranosyl-(1→2)-beta-D-galactopyranoside
15	10349838	$C_{32}H_{36}O_{18}$	708.6	Kalambroside-A

Cytoscape software (version 3.10.3). The resulting PPI network comprised 185 nodes and 3073 edges, with an average number of neighbours of 33.222, a network density of 0.181, and a heterogeneity score of 0.811, as illustrated in Fig. S3 and S4. Among these, the top five hub proteins based on degree centrality were AKT1, TP53, TNF, ALB, and EGFR (detailed in Table S3). Cluster analysis was conducted to identify significant modules within the network using the MCODE algorithm, resulting in four distinct modules. The characteristics of these modules are presented in Table 4.

GO analysis and KEGG pathway enrichment analysis. David go analysis was done and STRING web tool was used to map the CC, BP and MF enrichment. The number of cellular components (CC), molecular functions (MF), and biological processes (BP) were analyzed. According to the *p*-value (FDR), the top 5 CCs were: membrane raft, cell periphery, plasma membrane, vesicle, and cytoplasm. The enriched BPs included: response to organic substance, response to chemical, response to stimulus, response to oxygen-containing compound, and cellular response to chemical stimulus. The top 5 MFs were: catalytic activity, protein binding, binding, ion binding, and enzyme binding. All the top 10 terms of CC, BP, and MF are included in Fig. S5.

The different pathways enriched were identified through KEGG pathway enrichment analysis. We used DAVID GO for enrichment analysis to identify the pathways and obtained 204 signaling pathways. Among the top 20 pathways, sorted based on *p*-values from smallest to largest, the results are plotted in the form of a bar graph as shown in Fig. S6. The analysis revealed that key targets are enriched in pathways such as pathways in cancer, PI3K–AKT signaling pathway, estrogen signaling pathway, PD-1 checkpoint pathways in cancer, IL-17 signaling pathway, and Th17 cell differentiation. KEGG analysis shows that most of the common genes are involved in multiple pathways associated with cancer, providing valuable insights into the anti-cancer potential of *K. laciniata* compounds through ABC transporter interaction. Fig. S7.

Relationship between active compounds–potential therapeutic target, and critical pathways involved. To further analyze the relationship between active compounds, potential targets, and critical pathways involved, we constructed a network using Cytoscape, as shown in Fig. S8. The network comprises 465 nodes and 1515 edges, with an average of 6.516 neighbours per node. Among the compounds, kaempferol derivatives showed the highest degree score (108), followed by other compounds such as rutin, stigmasterol, closely related to potential targets and possess the highest degree value of 100. The genes AKT1, and TP53 are considered important in this context. Consequently, these compounds were selected for docking with the key targets using Schrodinger software.

Molecular docking. The protein 3D structures in PDB format were downloaded from Protein Data Bank and used for molecular docking. The PDB IDs of ABC transporters retrieved were, used in *in silico* docking studies conducted using Schrödinger Maestro software highlighted the significance of specific compounds in the anti-cancer activity of KLM. The docking studies involved three ABC transporters–P-glycoprotein (P-gp), Breast Cancer Resistance Protein (BCRP), and Multidrug Resistance Protein 1 (MRP1) as well as four hub genes: AKT1, TNF-alpha, ALB, and TP53. Among the various compounds tested, quercetin 3-(2-glucosylrhamnoside), kaempferol-3-*O*-glucoside-3-rhamnoside, and quercetin 3-*O*-beta-D-xylopyranosyl-(1→2)-beta-D-galactopyranoside performed exceptionally well, demonstrating strong binding affinities (varying docking scores of −7 to −16) with the targeted ABC transporter proteins and hub genes. The docking results revealed that several ligands exhibited strong binding affinities *i.e.* AKT1 with −13.1123 shows the binding score of −13.112, BCRP with quercetin 3-(2-glucosylrhamnoside) with the binding score of −16.228, showed significant docking scores which were displayed in the heatmap displayed in Fig. 2 along with their 2D and 3D images are shown in Fig. 3.

These results underscore the importance of quercetin and kaempferol derivatives in mediating the drug resistance effects associated with ABC transporters. Overall, the findings from

Open Access Article. Published on 13 February 2026. Downloaded on 4/5/2026 6:05:47 PM.
This article is licensed under a Creative Commons Attribution-NonCommercial 3.0 Unported Licence.

Table 4 Modules of the protein–protein interactions network of common targets of ABC transporter-associated targets modulated by KLM

S. no.	Module	MCODE score	Nodes	Edges
1	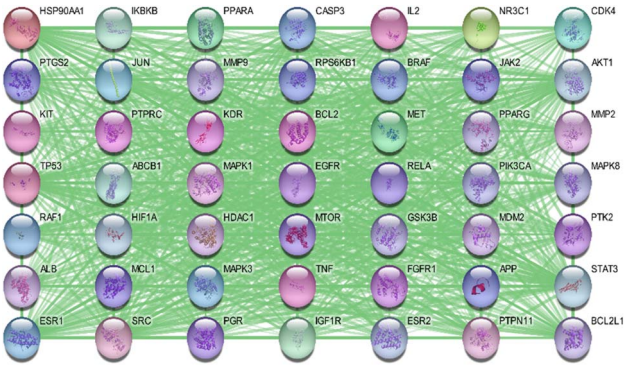	39.5	49	948
2	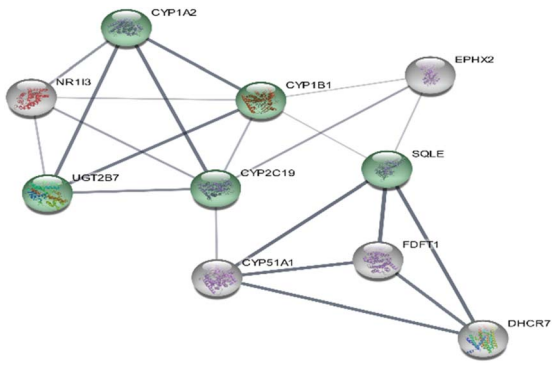	4.6	10	21
3	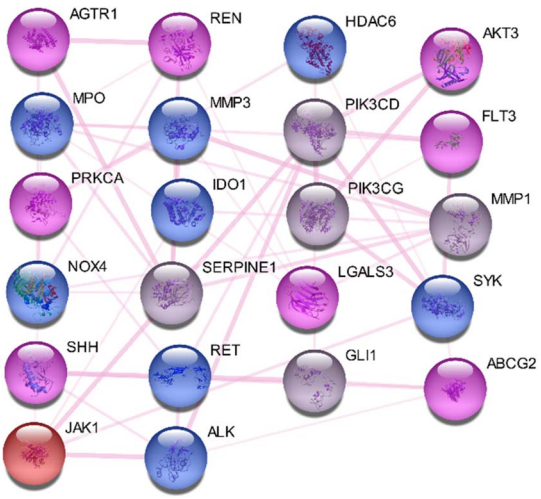	4.5	22	48
4	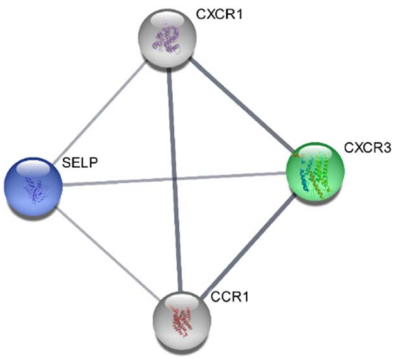	4	4	6

© 2026 The Author(s). Published by the Royal Society of Chemistry

Open Access Article. Published on 13 February 2026. Downloaded on 4/5/2026 6:05:47 PM. This article is licensed under a Creative Commons Attribution-NonCommercial 3.0 Unported Licence.

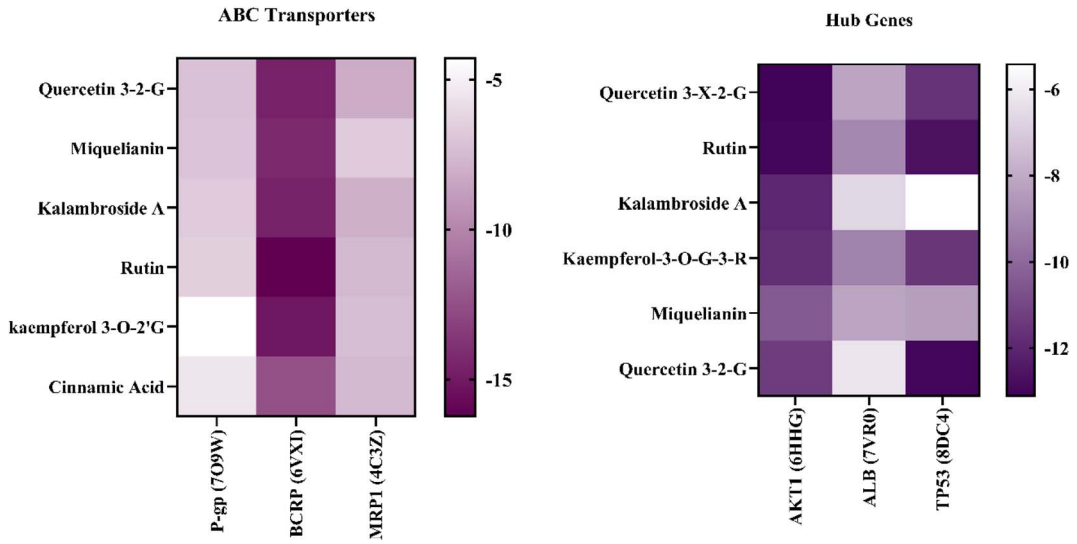

Fig. 2 Interaction profiles of ABC transporter proteins and Hub genes with high-affinity KLM phytocompounds.

this study provide a solid basis for further investigation into the pharmacological applications of quercetin and kaempferol derivatives derived from *Kalanchoe laciniata* in multi-drug resistance treatment.

Dynamics simulation

Molecular dynamic simulation studies. Molecular dynamics simulations were performed for four target proteins – P-gp, BCRP, MRP1, and AKT1 – using their best docked ligand

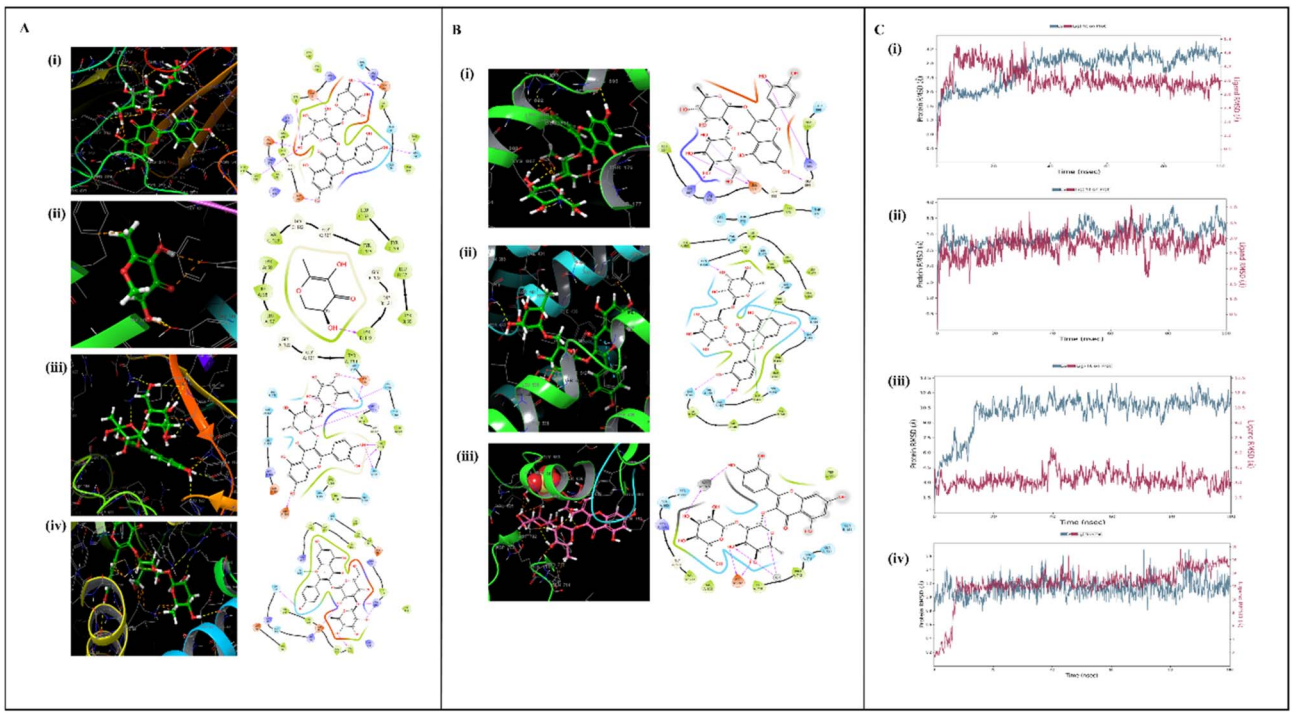

Fig. 3 2D and 3D interaction profiles and molecular dynamics stability analysis of selected ABC transporters and hub protein–phytocompound complexes. Panels (A) (i–iv) show the 2D and 3D interaction maps of the top four hub proteins with their respective highest-affinity ligands: (i) AKT1–quercetin 3-*O*-β-D-xylopyranosyl-(1→2)-β-D-galactopyranoside, (ii) TNFA–2,3-dihydro-3,5-dihydroxy-6-methyl-4*H*-pyran-4-one, (iii) TP53–quercetin 3-(2-glucosylrhamnoside), and (iv) ALB–kaempferol-3-*O*-glucoside-3-rhamnoside. Panels (B) (i–iii) depict the 2D and 3D binding conformations of three ABC transporters with their top-ranked ligands: (i) P-gp–quercetin 3-(2-glucosylrhamnoside), (ii) BCRP–rutin, and (iii) MRP1–quercetin 3-(2-glucosylrhamnoside). Panels (C) (i–iv) present the RMSD trajectories over 100 ns molecular dynamics simulations for selected protein–ligand complexes: (i) AKT1–quercetin 3-*O*-β-D-xylopyranosyl-(1→2)-β-D-galactopyranoside, (ii) BCRP–rutin, (iii) P-gp–quercetin 3-(2-glucosylrhamnoside), and (iv) MRP1–quercetin 3-(2-glucosylrhamnoside), illustrating the structural stability and dynamic behavior of the complexes during simulation.

© 2026 The Author(s). Published by the Royal Society of Chemistry

Open Access Article. Published on 13 February 2026. Downloaded on 4/5/2026 6:05:47 PM. This article is licensed under a Creative Commons Attribution-NonCommercial 3.0 Unported Licence.

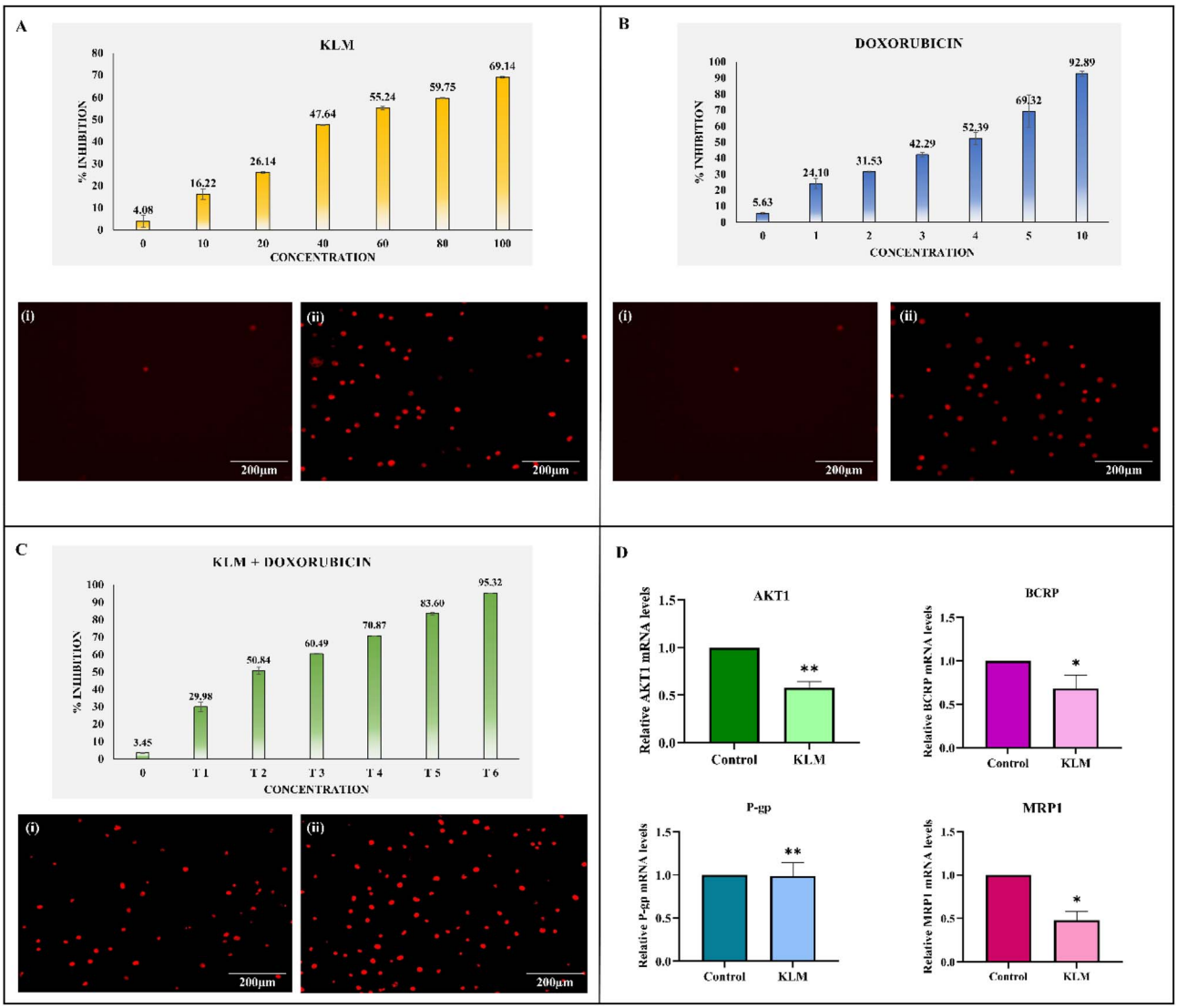

Fig. 4 Panel (A) illustrates the dose-dependent cytotoxic effect of KLM on MDA-MB-231 cells as determined by the MTT assay following 24 h treatment (10–100 µg mL^{-1}), along with representative propidium iodide (PI)-stained fluorescence images of untreated control cells and cells treated with the IC_{50} concentration (60.55 µg mL^{-1}), indicating reduced cell viability. Panel (B) shows the cytotoxic response of doxorubicin (1–10 µg mL^{-1}) evaluated by MTT assay after 24 h exposure, together with PI-stained images of control cells and cells treated with the IC_{50} concentration (4.10 µg mL^{-1}), demonstrating decreased cell survival. Panel (C) depicts the cytotoxic effect of the KLM–doxorubicin combination on MDA-MB-231 cells assessed by the MTT assay, with corresponding PI-stained images of T2-treated cells showing partial inhibition and T5-treated cells showing a pronounced reduction in viable cells. In panels (A–C), data are presented as mean ± SD of triplicate experiments, and statistical significance was determined using one-way ANOVA. Panel (D) shows the relative mRNA expression levels of AKT1, BCRP, P-gp, and MRP1 following KLM treatment, determined by quantitative real-time PCR and normalized to β-actin. Data are presented as mean ± SD of duplicate experiments, with statistical significance indicated relative to the control (*$p < 0.05$; **$p < 0.01$).

complexes selected based on docking scores and ADMET properties. Protein backbone RMSD analysis showed that the complexes BCRP–rutin, MRP1–quercetin 3-(2-glucosylrhamnoside), and AKT1–quercetin 3-*O*-β-D-xylopyranosyl-(1→2)-β-D-galactopyranoside achieved stability within the first 10 ns and remained stable throughout the 100 ns simulation period, with fluctuations within the acceptable range of 0.5–4 Å. In contrast, the P-gp–quercetin 3-(2-glucosylrhamnoside) complex exhibited consistently higher RMSD values, suggesting weak or unstable binding and failure to form a stable complex during the simulation. These findings indicate favorable binding stability for selected ligands with BCRP, MRP1, and AKT1, but poor interaction with P-gp, which are displayed in Fig. 3.

Root mean square fluctuation (RMSF) analysis revealed that C-terminal regions of MRP1, P-gp, and AKT1 displayed higher flexibility compared to the N-terminal regions, which remained relatively stable, suggesting greater structural rigidity at the N-terminus. P-gp showed a pronounced peak around residue 600, indicating a highly flexible loop or exposed region, while AKT1 displayed notable fluctuations near residues 50, 250, and 300, reflecting dynamic loop regions. Protein–ligand interaction profiling further demonstrated that hydrogen bonding and

© 2026 The Author(s). Published by the Royal Society of Chemistry

Open Access Article. Published on 13 February 2026. Downloaded on 4/5/2026 6:05:47 PM. This article is licensed under a Creative Commons Attribution-NonCommercial 3.0 Unported Licence.

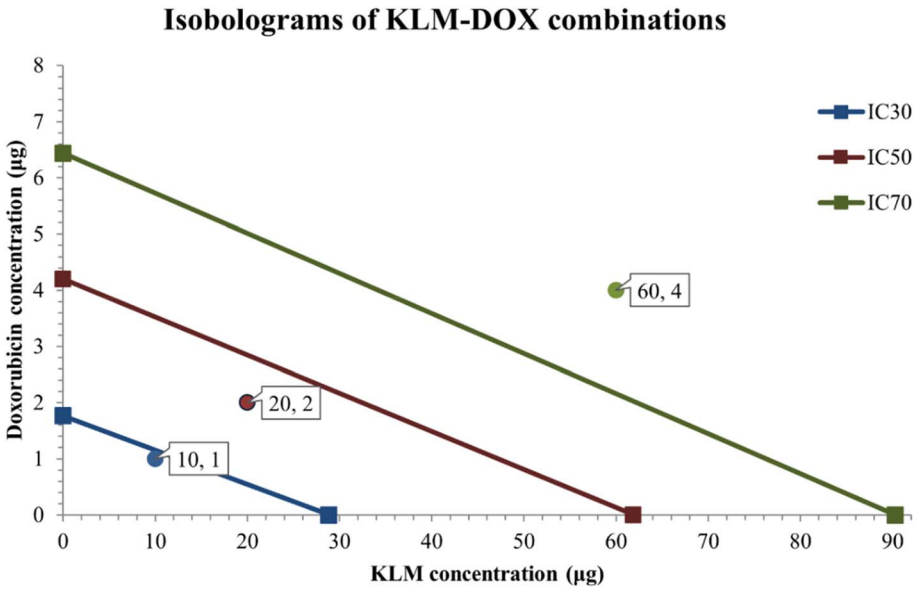

Fig. 5 Isobologram analysis of the interaction between KLM and doxorubicin in MDA-MB-231 Cells.

hydrophobic interactions were the dominant stabilizing forces across complexes, with AKT1 and BCRP showing strong interaction profiles, including water bridges and ionic interactions. Two-dimensional interaction maps confirmed persistent contacts between key residues and ligands, supporting the stability and functional relevance of these complexes during simulation.

Effects of KLM and doxorubicin on the cytotoxicity of MDA-MB-231 cell line. The cytotoxic activity of the methanolic extract of *Kalanchoe laciniata* (KLM) against the MDA-MB-231 human breast cancer cell line was evaluated using the MTT assay. Cells were treated with increasing concentrations of the extract (10–100 µg mL^{-1}) for 24 hours, and the percentage of cell inhibition was determined. The results demonstrated a clear dose-dependent increase in cytotoxicity, with the extract showing approximately 16.22% inhibition at 10 µg mL^{-1}, 26.14% at 20 µg mL^{-1}, 47.64% at 40 µg mL^{-1}, 55.24% at 60 µg mL^{-1}, 59.74% at 80 µg mL^{-1}, and reaching 69.14% inhibition at 100 µg mL^{-1}. The calculated IC_{50} value of the KLM extract was found to be 60.55 µg mL^{-1}, indicating good cytotoxic activity against MDA-MB-231 cells in a concentration-dependent manner, displayed in Fig. 4A.

For comparison, the standard drug doxorubicin (positive control) exhibited a strong cytotoxic response. The results revealed a concentration-dependent increase in cytotoxicity, with percentage inhibitions of approximately 5.63%, 24.10%, 31.52%, 42.29%, 52.39%, 69.32%, and 92.89% at 0, 1, 2, 3, 4, 5, and 10 µg mL^{-1}, respectively. The calculated IC_{50} value of doxorubicin was 4.10 µg mL^{-1}, indicating potent cytotoxic activity against MDA-MB-231 cells Fig. 4B. The methanolic extract of *Kalanchoe laciniata* showed concentration-dependent cytotoxicity in normal RIN-5F cells (IC_{50} = 242.17 µg mL^{-1}), which was substantially higher than that observed in MDA-MB-231 breast cancer cells (IC_{50} = 60.55 µg mL^{-1}), indicating a favorable degree of cancer-selective toxicity (Fig. S12).

Cytotoxic effect of KLM in combination with doxorubicin on MDA-MB-231 cells. The combination treatment of *Kalanchoe laciniata* methanolic extract (KLM) with doxorubicin exhibited a dose-dependent increase in cytotoxicity against MDA-MB-231 breast cancer cells. The percentage of cell growth inhibition increased progressively from 3.45% (control) to 29.98% (T1), 50.84% (T2), 60.49% (T3), 70.87% (T4), 83.60% (T5), and 95.32% (T6). The highest inhibition (95.32%) was observed at the maximum tested concentration, shown in Fig. 4C.

Isobologram analysis of KLM–doxorubicin combinations demonstrated a concentration- and effect-level-dependent interaction pattern. At IC_{30} and IC_{50}, the experimental combination points were positioned below their respective additivity

Table 5 Chou–Talalay based combination index analysis of KLM and doxorubicin in MDA-MB-231 cells

% Inhibition	C_A (µg ml^{-1})	C_B (µg ml^{-1})	IC_A (µg ml^{-1})	IC_B (µg ml^{-1})	Combination index	Synergy or antagonism
29.979	10	1	28.79443	1.76507	0.913837	Synergy
50.844	20	2	61.88815	4.201118	0.799231	Synergy
60.486	40	3	77.17934	5.32685	1.081454	Additive
70.866	60	4	93.64249	6.538744	1.252469	Antagonism
83.603	80	5	113.8447	8.025826	1.325701	Antagonism
95.320	100	10	132.4285	9.393819	1.819656	Antagonism

© 2026 The Author(s). Published by the Royal Society of Chemistry

Open Access Article. Published on 13 February 2026. Downloaded on 4/5/2026 6:05:47 PM. This article is licensed under a Creative Commons Attribution-NonCommercial 3.0 Unported Licence.

lines, indicative of synergistic interactions (Fig. 5). Consistent with the Chou–Talalay median-effect principle, this positioning corresponds to Combination Index (CI) values < 1, reflecting achievement of equivalent cytotoxic effects at lower-than-predicted doses relative to dose additivity. Such synergism suggests that KLM enhances doxorubicin efficacy at low to moderate effect levels, supporting a chemosensitizing role that may involve modulation of drug-resistance-associated mechanisms. In contrast, the IC_{70} combination point was located above the additivity line, corresponding to CI values > 1 and indicating an antagonistic interaction at higher effect levels (Table 5). This attenuation of synergy at elevated concentrations may be attributed to target saturation or activation of compensatory cellular responses, a phenomenon frequently reported in phytochemical-based combination studies.[41,42] Collectively, the concordance between isobologram positioning and Chou–Talalay CI interpretation indicates that KLM exhibits optimal synergistic potential with doxorubicin at IC_{30}–IC_{50} levels, supporting its role as a dose-modulating adjuvant rather than a high-dose cytotoxic agent.

Quantitative real-time PCR analysis demonstrated that KLM treatment significantly altered the mRNA expression of AKT1 and ABC transporter genes, including BCRP, P-gp, and MRP1, compared with the untreated control group (Fig. 4D). Notably, KLM treatment was associated with a significant down-regulation of AKT1, BCRP, and MRP1 transcript levels. In contrast, the expression of P-gp did not show a statistically significant increase under the experimental conditions employed. These results indicate that KLM influences the transcriptional levels of selected genes implicated in cell survival and drug resistance pathways. These findings suggest that KLM modulates AKT signaling and selectively influences the expression of multidrug resistance transporters, indicating its potential role in regulating cancer cell survival and drug resistance mechanisms.

Discussion and conclusion

Discussion

Multidrug resistance (MDR) mediated by ATP-binding cassette (ABC) transporters remains a major challenge in effective cancer chemotherapy. In this study, *Kalanchoe laciniata* was investigated as a potential source of MDR-modulating phytochemicals through an integrated approach combining phytochemical profiling, network pharmacology, molecular docking, and experimental validation. Our findings provide mechanistic evidence that flavonoid glycosides from *K. laciniata*, particularly quercetin and kaempferol derivatives, target key regulators of drug resistance and cancer cell survival[43]

Phytochemical analyses consistently identified quercetin- and kaempferol-based glycosides as major constituents of the KLM. Network pharmacology analysis revealed that these compounds converge on ABC transporters, including P-glycoprotein (P-gp), breast cancer resistance protein (BCRP), and multidrug resistance protein-1 (MRP1), as well as survival-associated hub genes such as AKT1 and TP53. Enrichment of the PI3K–AKT signaling pathway and drug resistance-related pathways highlight a coordinated mechanism through which *K. laciniata* phytochemicals may regulate both transporter activity and intracellular survival signaling. This multi-target action aligns with current concepts that MDR arises from interconnected molecular networks rather than single-gene alterations.[44,45]

Molecular docking and molecular dynamics simulations further supported these findings by demonstrating stable interactions between quercetin and kaempferol derivatives and ABC transporters, particularly BCRP and MRP1. These interactions involved key residues within the transporter binding pockets, suggesting potential competitive or allosteric inhibition of efflux activity. Molecular dynamics simulations (100 ns) revealed that the BCRP–rutin, MRP1–quercetin 3-(2-glucosylrhamnoside), and AKT1–quercetin 3-*O*-β-D-xylopyranosyl-(1→2)-β-D-galactopyranoside complexes rapidly achieved structural stability within the first 10 ns and remained stable throughout the simulation (RMSD 0.5–4 Å), whereas the P-gp–quercetin 3-(2-glucosylrhamnoside) complex exhibited higher RMSD fluctuations, indicating weak and unstable binding.[46] Notably, strong interactions with BCRP are of particular interest, as BCRP-mediated drug efflux contributes significantly to resistance against several clinically used chemotherapeutics and remains less extensively explored than P-gp.[15]

Additionally, interactions with AKT1 suggest that these flavonoids may indirectly regulate transporter expression through suppression of pro-survival signaling pathways.[43] It is also important to note that *in silico* prediction tools are biased toward well-characterized targets and pathways, which may limit identification of less-studied or context-specific interactions. Accordingly, the predicted networks should be interpreted as hypothesis-generating. To partially address this limitation, experimental validation was performed using qPCR analysis of selected key target genes, providing preliminary biological support for the network pharmacology predictions.

Quantitative real-time PCR analysis demonstrated that KLM treatment significantly downregulated the mRNA expression of AKT1, BCRP, and MRP1, providing experimental support for selected targets predicted through network pharmacology and molecular docking.[47] Suppression of AKT1 is particularly noteworthy given its established role in promoting cell survival, inhibiting apoptosis, and regulating ABC transporter expression. In contrast, P-gp (ABCB1) expression did not show significant transcriptional modulation, which is consistent with the relatively lower stability observed for the P-gp–ligand complex during molecular dynamics simulations. Taken together, these findings suggest that KLM-mediated MDR modulation may preferentially involve AKT signaling, BCRP, and MRP1, rather than broad or nonspecific inhibition of all ABC transporters. Accordingly, the *in silico* and qPCR data were interpreted in a complementary and cautious manner, highlighting target selectivity rather than uniform ABC transporter inhibition. While qPCR analysis provided initial experimental support for the *in silico* predicted modulation of ABC transporter related genes, the absence of protein expression and functional activity assays represents a limitation of the present study. Future investigations incorporating transporter activity

© 2026 The Author(s). Published by the Royal Society of Chemistry

Open Access Article. Published on 13 February 2026. Downloaded on 4/5/2026 6:05:47 PM. This article is licensed under a Creative Commons Attribution-NonCommercial 3.0 Unported Licence.

assays and protein-level validation will be essential to confirm the functional relevance of these findings.

Functionally, KLM exhibited selective cytotoxicity toward MDA-MB-231 breast cancer cells compared with normal RIN-5F cells, indicating a favorable *in vitro* selectivity profile. In addition, the synergistic interaction observed between KLM and doxorubicin at defined effect levels suggests enhanced cytotoxic efficacy when used in combination. While the observed synergy is consistent with reduced ABC transporter-mediated drug efflux, confirmation of direct transporter activity modulation will require dedicated efflux assays in future studies. Taken together, the cytotoxicity and combination data provide preliminary biological context for the molecular and transcriptional observations, supporting a hypothesis of selective MDR modulation by KLM under *in vitro* conditions.

Conclusion

Collectively, this study provides integrative evidence that *Kalanchoe laciniata* exerts a multi-targeted influence on MDR-associated pathways, involving modulation of ABC transporter-related genes and survival signaling at the *in silico* and transcriptional levels. The combined computational and *in vitro* findings identify quercetin and kaempferol derived constituents as potential chemosensitizing candidates, rather than confirmed therapeutic agents. While these results highlight the promise of *K. laciniata* as an adjunct in combination chemotherapy, comprehensive validation through functional efflux assays, protein-level analysis, and *in vivo* pharmacokinetic and efficacy studies will be essential before proceeding to translational and clinical studies.

Author contributions

Anish Ruban S.: writing – original draft, conceptualization, methodology, investigation; Francis Jegan Raj: formal analysis, data curation; Vetri Velavan Sundararajan: validation, resources, writing – review & editing; Parimelazhagan Thangaraj: writing – review, supervision.

Conflicts of interest

The authors declare no conflict of interest.

Data availability

No software or code have been included and all data generated has been included in either the manuscript or supplementary data.

Supplementary information (SI) is available. See DOI: https://doi.org/10.1039/d5ra09649a.

Acknowledgements

We thank CSIR-UGC, and the Department of Botany, Bharathiar University, Coimbatore, for the support provided to undertake this study. This work was funded by CSIR UGC (NTA Ref. No: 211610197248), and the Department of Botany, Bharathiar University, Coimbatore.

References

1 J. M. Fernandes, L. M. Cunha, E. P. Azevedo, E. M. G. Lourenço, M. F. Fernandes-Pedrosa and S. M. Zucolotto, *Rev. Bras. Farmacogn.*, 2019, **29**, 529–558.
2 S. El Abdellaoui, E. Destandau, A. Toribio, C. Elfakir, M. Lafosse, I. Renimel, P. André, P. Cancellieri and L. Landemarre, *Anal. Bioanal. Chem.*, 2010, **398**, 1329–1338.
3 E. R. D. de Araújo, G. C. B. Guerra, D. F. de Souza Araújo, A. A. de Araújo, J. M. Fernandes, R. F. de Araújo Júnior, V. C. da Silva, T. G. de Carvalho, L. de Santis Ferreira and S. M. Zucolotto, *Int. J. Mol. Sci.*, 2018, **19**(5), 1265.
4 A. Rudzińska, P. Juchaniuk, J. Oberda, J. Wiśniewska, W. Wojdan, K. Szklener and S. Mańdziuk, *Nutrients*, 2023, **15**, 1896.
5 D. M. Kopustinskiene, V. Jakstas, A. Savickas and J. Bernatoniene, *Nutrients*, 2020, **12**(2), 457.
6 H. Patel, Z. X. Wu, Y. Chen, L. Bo and Z. S. Chen, *Mol. Biomed.*, 2021, **2**, 27.
7 X. Wang, H. Zhang and X. Chen, *Cancer Drug Resist.*, 2019, **2**, 141–160.
8 A. E. van Herwaarden and A. H. Schinkel, *Trends Pharmacol. Sci.*, 2006, **27**(1), 10–16.
9 R. W. Robey, K. M. Pluchino, M. D. Hall, A. T. Fojo, S. E. Bates and M. M. Gottesman, *Nat. Rev. Cancer*, 2018, **18**(7), 452–464.
10 K. Katayama, K. Masuyama, S. Yoshioka, H. Hasegawa, J. Mitsuhashi and Y. Sugimoto, *Cancer Chemother. Pharmacol.*, 2007, **60**, 789–797.
11 H. Xiao, Y. Zheng, L. Ma, L. Tian and Q. Sun, *Front. Pharmacol*, 2021, **12**, 648407.
12 M. E. Hernández-Caballero, J. A. Sierra-Ramírez, R. Villalobos-Valencia and E. Seseña-Méndez, *Molecules*, 2022, **27**, 6425.
13 D. C. Faustino, N. N. das Chagas Lima, K. J. Allahdadi and L. C. Pinto, *RPS Pharm. Pharmacol. Rep.*, 2022, **1**, rqac009.
14 F. B. Barlas, *J. Radiat. Res. Appl. Sci.*, 2023, **16**, 100612.
15 A. Singh, S. K. Patel, P. Kumar, K. C. Das, D. Verma, R. Sharma, T. Tripathi, R. Giri, N. Martins and N. Garg, *J. Biomol. Struct. Dyn.*, 2022, **40**, 4507–4515.
16 G. An, J. Gallegos and M. E. Morris, *Drug Metab. Dispos.*, 2011, **39**, 426–432.
17 S. A. Ruban, F. J. Raj and P. Thangaraj, *Biochim. Biophys. Acta, Rev. Cancer*, 2025, **1880**, 189349.
18 A. A. Jovanović, V. B. Đorđević, G. M. Zdunić, D. S. Pljevljakušić, K. P. Šavikin, D. M. Gođevac and B. M. Bugarski, *Sep. Purif. Technol.*, 2017, **179**, 369–380.
19 F. J. Raj, G. Jagadeesan, B. M. Paul, P. Thangaraj and R. Kilimas, *Appl. Biochem. Biotechnol.*, 2023, **195**, 6790–6808.
20 K. Gurning, H. A. Simanjuntak, H. Purba, R. F. R. Situmorang, L. Barus and S. Silaban, *J. Phys., Conf. Ser.*, 2021, **1811**, 012121.
21 A. Mehmood, S. Javid, M. F. Khan, K. S. Ahmad and A. Mustafa, *BMC Chem.*, 2022, **16**, 1–10.
22 İ. Gulcin and S. H. Alwasel, *Processes*, 2023, **11**, 2248.

© 2026 The Author(s). Published by the Royal Society of Chemistry

Open Access Article. Published on 13 February 2026. Downloaded on 4/5/2026 6:05:47 PM. This article is licensed under a Creative Commons Attribution-NonCommercial 3.0 Unported Licence.

23 A. Mehta, *Vegetos*, 2023, **36**, 1570–1575.
24 H. Aziz, A. Saeed, F. Jabeen, M. A. Khan, A. Ur Rehman, M. Q. Khan and M. Saleem, *J. Mol. Struct.*, 2023, **1278**, 134924.
25 J. Rumpf, R. Burger and M. Schulze, *Int. J. Biol. Macromol.*, 2023, **233**, 123470.
26 R. Apak, A. Calokerinos, S. Gorinstein, M. A. Segundo, D. B. Hibbert, I. Gülçin, S. D. Çekiç, K. Güçlü, M. Özyürek, S. E. Çelik, L. M. Magalhães and P. Arancibia-Avila, *Pure Appl. Chem.*, 2022, **94**, 87–144.
27 F. P. Nonglang, A. Khale and S. Bhan, *Future J. Pharmaceut. Sci.*, 2022, **8**, 1–12.
28 J. M. Dinore, H. S. Patil, B. S. Dobhal and M. Farooqui, *Nat. Prod. Res.*, 2022, **36**, 5631–5637.
29 L. Zhao, H. Zhang, N. Li, J. Chen, H. Xu, Y. Wang and Q. Liang, *J. Ethnopharmacol.*, 2023, **309**, 116306.
30 M. Kohl, S. Wiese and B. Warscheid, *Methods Mol. Biol.*, 2011, **696**, 291–303.
31 *SRplot-Science and Research online plot*, https://www.bioinformatics.com.cn/srplot, accessed 31 May 2025.
32 *RCSB PDB: Homepage*, https://www.rcsb.org/, accessed 31 May 2025.
33 A. Lakshmanan, B. Balasubramanian, V. Maluventhen, A. Malaisamy, R. Baskaran, W. C. Liu and M. Arumugam, *Appl. Sci.*, 2022, **12**, 13010.
34 S. Menaga and N. Geetha, *Next Res.*, 2025, **2**, 100500.
35 S. K. Mandal, B. K. Kumar, P. K. Sharma, S. Murugesan and P. R. Deepa, *Comput. Biol. Med.*, 2022, **147**, 105796.
36 N. S. Natesh, M. Arumugam and G. Karanam, *Mol. Biol. Rep.*, 2018, **45**(6), 2641–2651.
37 T. C. Chou, *Cancer Res.*, 2010, **70**, 440–446.
38 G. Karanam and M. K. Arumugam, *Mol. Biol. Rep.*, 2020, **47**(5), 3347–3359.
39 M. Suriyakanthan and G. Natesan, *RSC Adv.*, 2025, **15**, 49399–49417.
40 S. Menaga and N. Geetha, *Next Re.*, 2025, 100500.
41 L. K. Caesar and N. B. Cech, *Nat. Prod. Rep.*, 2019, **36**, 869–888.
42 N. Chaachouay, *Drugs Drug Candidates*, 2025, **4**, 4.
43 N. S. Yarla, *J. Mar. Sci. Res. Dev.*, 2013, **4**(1), DOI: 10.4172/2155-9910.1000e123.
44 R. Liu, Y. Chen, G. Liu, C. Li, Y. Song, Z. Cao, W. Li, J. Hu, C. Lu and Y. Liu, *Cell Death Dis.*, 2020, **11**, 1–12.
45 S. A. Mirzaei, F. Dinmohammadi, A. Alizadeh and F. Elahian, *Life Sci.*, 2019, **235**, 116825.
46 S. A. Hollingsworth and R. O. Dror, *Neuron*, 2018, **99**(6), 1129–1143.
47 G. Ramarajyam, R. Murugan and S. Rajendiran, *Hum. Gene*, 2024, **42**, 201328.

© 2026 The Author(s). Published by the Royal Society of Chemistry